Archaeomagnetic results on three Early Iron Age salt-kilns from Moyenvic (France)

Gwenaël Hervé, Elisabeth Schnepp, Annick Chauvin, Philippe Lanos, Norbert Nowaczyk

Geophysical Journal International

Geophys. J. Int. (2011) **185,** 144–156 doi: 10.1111/j.1365-246X.2011.04933.x

Archaeomagnetic results on three Early Iron Age salt-kilns from Moyenvic (France)

Gwenaël Hervé,[1,3] Elisabeth Schnepp,[2] Annick Chauvin,[3] Philippe Lanos[1,3] and Norbert Nowaczyk[4]

[1] *Centre de Recherches en Physique Appliquée à l'Archéologie, UMR* 5060*, Université de Bordeaux* 3*, CNRS, et UMR* 6118*, Université de Rennes* 1*, CNRS, Campus de Beaulieu, CS* 74205*,* 35042 *Rennes Cedex, France. E-mail: gwenael.herve@univ-rennes1.fr*

[2] *Paleomagnetic Laboratory Gams, Chair of Geophysics, University of Leoben, Gams* 45*, Frohnleiten* A8170*, Austria*

[3] *Géosciences-Rennes, UMR 6118, Université de Rennes* 1*, CNRS, Campus de Beaulieu, Bat* 15*, CS* 74205*, Rennes Cedex* 35042*, France*

[4] *GeoForschungsZentrum Potsdam, Section* 5.2*—Palaeoclimate & Landscape Evolution Helmholtz-Zentrum Potsdam Deutsches GeoForschungsZentrum GFZ Telegrafenberg Haus* C321*, Potsdam D-*14473*, Germany*

Accepted 2010 December 26. Received 2010 December 17; in original form 2010 June 23

SUMMARY

Variations of the Earth's magnetic field during the first millennium BC in western Europe remain poorly constrained, especially archaeointensity changes. Three salt-kilns (MOA, MOB and MOC) sampled in Moyenvic (Lorraine, eastern France) have been studied to provide new reference data. Each kiln has been dated by radiocarbon to originate from the Early Iron Age or Hallstatt period (between VIII and Vth Century BC). Rock magnetic experiments and hysteresis results suggest the predominance of pseudo-single domain (PSD) Ti-poor magnetite. Archaeomagnetic directions obtained by thermal and alternating field demagnetizations have high mean inclination (close to 70°) and declination (between 19 and 31°). A first set of classical Thellier–Thellier experiments was conducted on 46 samples with a laboratory field almost parallel to the direction of the characteristic remanent magnetization (ChRM). Only 24 of these specimens present a linear NRM–TRM plot. For other specimens, NRM–TRM plots are concave-up with positive pTRM checks. The very large dispersion observed between the determined palaeointensity values suggests some artefacts have not been fully recognized. A second set of Thellier experiments was conducted on 34 sister specimens with the laboratory field applied quasi-perpendicular to the ChRM. In these cases, mineralogical evolutions during heating and chemical remanent magnetization acquisitions have been clearly recognized, despite positive pTRM checks. The concave-up shapes of NRM–TRM plots appear mainly due to mineralogical alteration rather than to the presence of PSD–MD grains. For the entire set of samples the success rate of the palaeointensity determinations is very low with 80 per cent of the samples rejected. Nevertheless, reliable mean archaeointensities have been obtained for two of the three kilns (MOA, 80.1 ± 14.5 μT and MOB, 86.6 ± 6.9 μT at the latitude of Paris). The high field strength and the archaeomagnetic directions determined, combined with previous published data, provide further evidence for important changes of the Earth magnetic field in Europe during the first half of the first millennium BC. These large variations of the geomagnetic field during the Iron Ages indicate that archaeomagnetism is highly suitable for dating of structures from this period.

Key words: Archaeomagnetism; Magnetic field; Palaeointensity; Palaeomagnetic secular variation.

1 INTRODUCTION

Knowledge of the secular variation of the geomagnetic field in Western Europe has been considerably improved over recent years using archaeodirections (e.g. Gallet *et al.* 2002; Schnepp & Lanos 2005; Gomez-Paccard *et al.* 2006; Tema *et al.* 2006; Zananiri *et al.* 2007) as well as archaeointensities (Gomez-Paccard *et al.* 2008; Genevey *et al.* 2009, Schnepp *et al.* 2009). These new data have allowed considerable improvement in geomagnetic field models, on both global (ARCH3k, Korte *et al.* 2009) and regional (SCHA.DIF.3k, Pavon-Carrasco *et al.* 2009) scales. Archaeomagnetic dating has also become increasingly applicable in many European countries (Lanos 2004). In France and in Germany, directional secular variation curves cover, respectively, the last 2500 and 3000 yr. (Gallet

et al. 2002; Schnepp & Lanos 2005). However, the resolution of these curves only permits reliable archaeomagnetic dating of archaeological structures for the last two millennia. Archaeomagnetic dating is not yet sufficiently developed for the first millenium BC, that is, for the Iron Age.

The archaeointensity reference curve of Gomez-Paccard *et al.* (2008), established with western Europe data, covers only the last two millenia. Archaeointensity data for the first millennium BC were mainly obtained on sites from the Mediterranean area (Hill *et al.* 2007, 2008; Gallet *et al.* 2009) and eastern Europe (De Marco *et al.* 2008; Kovacheva *et al.* 2009). The number of data from northwestern Europe has to be increased to improve geomagnetic field model for this time period.

Moreover, all preliminary European data for the first millenium BC indicate very strong variations of the Earth's magnetic field, especially for declination and archaeointensity. Accordingly, this period appears very interesting for both understanding the evolution of the geomagnetic field and increasing the resolution of archaeomagnetic dating. As radiocarbon is not very precise for this period due to plateau effects on the dendrochronological calibration curve, archaeologists need another effective chronometric dating method. The aim of this study is to provide new reference data contributing to the French and German databases for the first millenium BC. It represents a new step to build secular variation curves useful for archaeomagnetic dating.

2 ARCHAEOLOGICAL CONTEXT

The village of Moyenvic is located in the Seille Valley, in the Lorraine region (eastern France, Fig. 1). The Seille valley is known as the most important centre of salt production in Northern Europe during the Early Iron Age (Bertaux 1987). Because of leaching of Triassic evaporitic layers, all springwaters in the area present a high salinity. Salt was produced in kilns during the Early Iron Age by the 'briquetage' technique (Daire 2003), which begins with an evaporation step, followed by the agglomeration of salt crystals at higher temperatures (700–750°C). It is in that latter step that kiln walls acquired a thermoremanent magnetization (TRM).

The survey excavation at the archaeological site of 'les Crôleurs' (48.80°N, 6.6°E) was undertaken by J.-D. Laffitte in 1999 and completed in 2001 (Laffitte 2002). 15 salterns and 40 salt-kilns were identified over 1 ha. Like most other kilns in this area, the three kilns we sampled, identified here as kilns MOA, MOB and MOC (Fig. 1) are underground and horseshoe shaped. Sampled kilns are

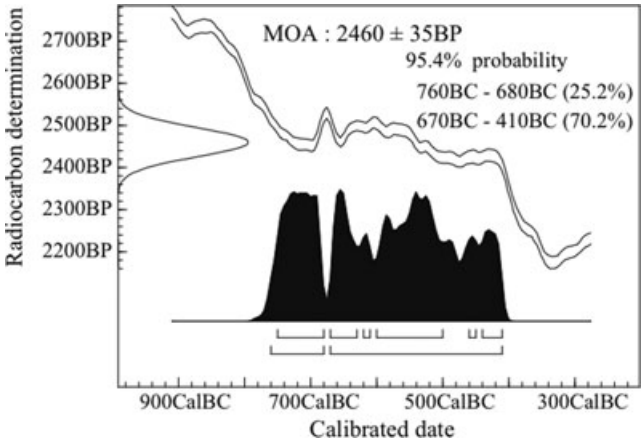

Figure 2. Example of radiocarbon dating on charcoal found in kiln MOA. Despite accurate uncalibrated ^{14}C-age, the presence of a plateau on the calibration curve during the Early Iron Age leads to large intervals on date estimate.

1.50–2.50 m long. Kiln walls seem to be have been well heated, particularly the central pillar.

The use period of the three kilns has been dated by radiocarbon analysis on charcoals found in each one of them. These analyses were carried out at the Groningen laboratory. Calibration of radiocarbon ages was realized with the Intcal04 curve (Reimer *et al.* 2004), using Oxcal software (v. 3.10, Bronk Ramsey 2005). Although the uncalibrated radiocarbon ages are precise, the calibrated date intervals are large, due to the long plateau in the calibration curve during the Early Iron Age (Fig. 2). Table 1 presents uncalibrated ages and calibrated dates at 95 per cent confidence for the three kilns. The absence of stratigraphic relationships between these kilns does not permit to reduce the intervals of calibrated dates.

3 SAMPLE PREPARATION AND MEASUREMENTS

29 large blocks samples on MOA, 23 on MOB and 18 on MOC were collected. They were oriented by placing plaster hats on the top surface (levelled horizontal using a bubble) and oriented using a magnetic compass and if possible a sun compass (MOB and MOC).

The block samples were very brittle and have been consolidated with waterglass. Two slices of 20 mm thickness, designated A and B, were cut from each block. One slice of each block has been

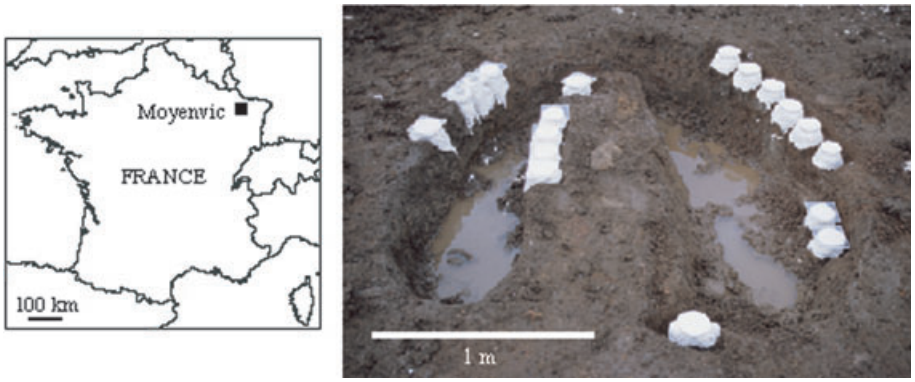

Figure 1. Location of the archaeological site Moyenvic les Crôleurs (48.780°N, 6.570°E) in Lorraine, Eastern France (left-hand side) and field photograph of horseshoe kiln MOC during sampling (right-hand side).

Table 1. Results of radiocarbon dating on charcoal sampled in each kiln. Calibrated ^{14}C dates are obtained with Oxcal software (Bronk Ramsey 2005) using the IntCal04 calibration curve (Reimer *et al.* 2004).

Kiln	Uncalibrated ^{14}C age (years BP)	Calibrated ^{14}C dates at 95.4 per cent confidence (CalBC)	^{14}C Age used in Fig. 13 (years BC)
MOA	2460 ± 35	[760; 680] and [670; 410]	585 ± 176
MOB	2550 ± 30	[800; 740], [690; 660] and [650; 540]	672 ± 129
MOC	2550 ± 50	[820; 510]	665 ± 155

further processed in the palaeomagnetic laboratory of Geosciences Rennes (France) and the other half was treated in the palaeomagnetic laboratory Grubenhagen of the LIAG (Germany) and in the palaeomagnetic laboratory Gams of the University of Leoben (Austria). Slices were cut into cubes of 8 cm^3 that were weighed.

Natural remanent magnetization (NRM) was measured with a 2G cryogenic magnetometer (Rennes, GAMS and Grubenhagen) or a Molspin spinner magnetometer (Rennes). Bulk susceptibility was measured with a Minikappa (Grubenhagen) or a Bartington MS2 (Rennes). In Rennes, thermomagnetic curves were obtained with a KLY3 Agico susceptibility meter with fitted furnace by heating–cooling cycles successively up to 350 and 650°C. In the palaeomagnetic laboratory of the GFZ Potsdam, hysteresis loop measurements have been carried out in a Princeton Micromag AGFM on small chips (a few milligrams) and for 11 additional chips isothermal remanent magnetization (IRM) acquisition and backfield curves were determined. First-order reversal curve (FORC) diagrams (Pike *et al.* 1999; Roberts *et al.* 2000) were measured at Potsdam.

Pilot alternating field demagnetizations were carried out using a Magnon demagnetizer up to 200 mT (Grubenhagen) or in a 2G-AF demagnetizer in line with the 2G cryogenic magnetometer. One specimen per sample was used, sometimes two. Thermal demagnetization was performed with a Magnon thermal demagnetizer (Grubenhagen) and a Magnetic Measurements Thermal Demagnetization (MMTD) oven (Rennes) for one specimen per sample and steps of 50°C from 150 to 600°C. A Thellier viscosity test (Thellier & Thellier 1944) was performed in Grubenhagen by storing two specimens per samples during 14 d with the $+Z$ and then the $-Z$ direction aligned with the Earth's magnetic field direction.

The classical Thellier–Thellier method (Thellier & Thellier 1959) with partial thermoremanent magnetization (pTRM) checks was used to estimate archaeointensity. Heating steps were realized in air in a MMTD oven in the laboratory of Rennes. At each temperature step, specimens were heated and cooled twice, first in a laboratory field $+F_{\rm Lab}$ and second in the opposite field $-F_{\rm Lab}$. Only specimens whose AF or thermally demagnetized sisters-specimens presented a single component of magnetization have been chosen. First, specimens of the three kilns were heated in a laboratory field of 60.0 μT applied along their Z-axis. In a second step, new Thellier experiments have been conducted with a laboratory field of 70 μT applied along the X-axis of the specimens. Eight to 12 temperature steps were performed from 100 to 560°C. Low-field susceptibility was measured after each heating step.

4 ROCK MAGNETIC RESULTS

4.1 Koenigsberger ratios

NRM intensity is plotted versus bulk susceptibility in Fig. 3(a) together with lines of increasing Koenigsberger ratios (Q defined as the ratio of NRM to the induced magnetization, a field of 40 A m^{-1} was used). In most cases, Q values are above 10 showing that these specimens acquired a TRM during the use of the kilns. For kiln MOA, the position of the block with respect to the combustion chamber is indicated by colour variations. Here most specimens (black crosses in Fig. 3) from blocks taken in the inner part of the kiln have higher NRM and susceptibility values comparable with those of the other kilns. The material of kiln MOA is very inhomogeneous and contains fragments of baked clay and some potsherds. Presumably this contributes to the large scatter in NRM intensities and in bulk susceptibilities. Generally, specimens from blocks sampled in the outer parts of the kiln (grey crosses) have Q-ratios below 5, suggesting that they acquired a weak partial thermoremanence.

4.2 Viscosity index

The viscosity index is defined as the ratio of the viscous remanent magnetization acquired within 14 days of storage in the laboratory field to that of the NRM (Thellier & Thellier 1944). Here it is mostly below 5 per cent (Fig. 3b), thus indicating little viscous contribution to a stable NRM. Only a very weak directional change of NRM directions is obtained after removing these small viscous components. No viscosity tests were performed on blocks MOA 12–29, because a partial thermoremanence is expected for these samples.

4.3 Magnetic stability

Figs 3(c) and (d) show the median destructive temperatures (MDT) and median destructive fields (MDF) for thermal and AF demagnetization, respectively. Usually the values of MDT lie above 350°C indicating high unblocking temperatures. Most MDF values are between 15 and 30 mT. These properties suggest the predominance of a magnetic carrier close to a magnetite composition.

4.4 Curie points

Furthermore, a Curie point close to 580 °C is observed on most of the 28 thermomagnetic curves (Fig. 4) suggesting that the predominant magnetic carrier is magnetite. However, in several specimens (e.g. MOB7 and MOB3), a Curie point around 200 °C is also observed. In addition, some specimens like MOB15 carry a ferrimagnetic phase with a Curie temperature of 620°C, which could indicate the presence of partially oxidized titanomagnetite or titanomaghemite. Most thermomagnetic curves are reversible for heating up to 350–400 °C but irreversible for heating up to 600 °C, especially for kiln MOC.

4.5 Hysteresis

In total, 24 IRM hysteresis curves have been measured with maximum fields of 1 T or 2 T. The results are plotted (Fig. 5) in a

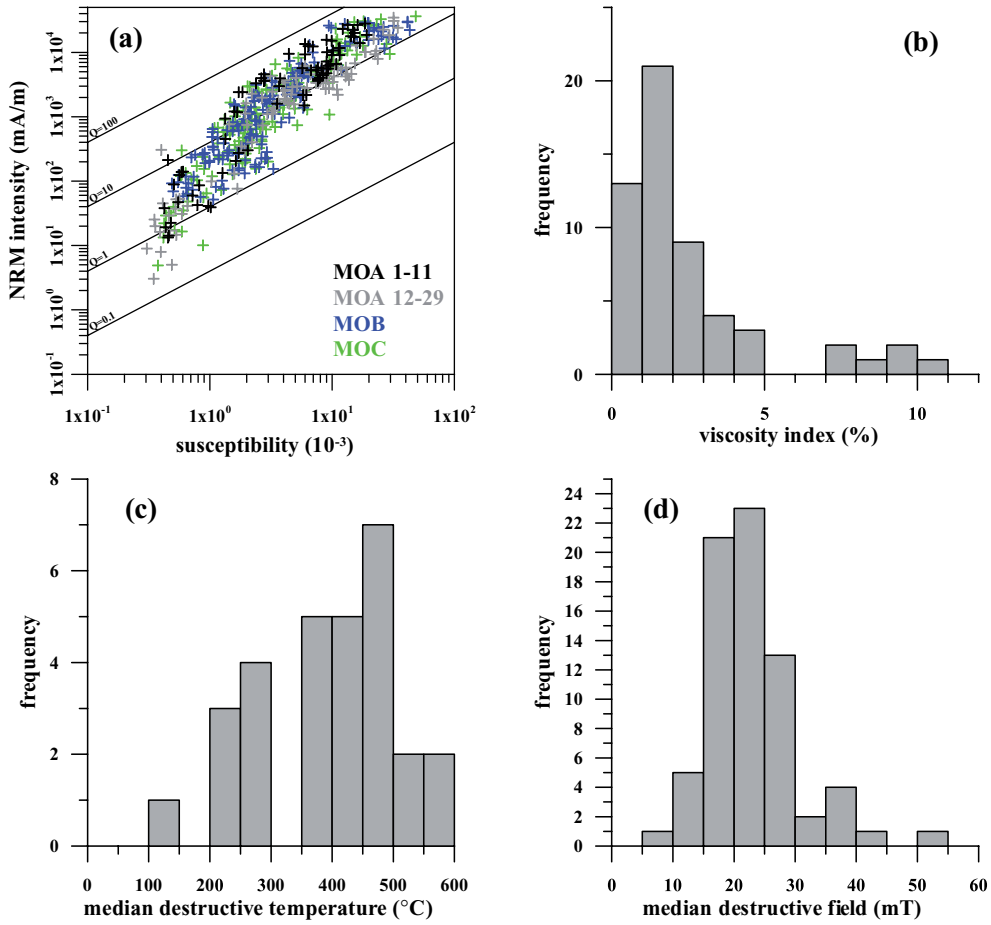

Figure 3. Rock magnetic parameters of the kilns. (a) Intensity of natural remanent magnetization (NRM) is plotted versus bulk susceptibility. Lines indicate constant Koenigsberger ratios between 0.1 and 100. Kiln MOA was divided into inner (1–11) and outer part (12–29). (b) Viscosity index obtained from experiments according to (Thellier & Thellier 1944). (c) Median destructive temperature. (d) Median destructive field obtained from thermal and alternating field demagnetization, respectively.

Day diagram (Day *et al.* 1977) showing that the domain state is pseudo-single domain (PSD). All specimens are far away from the single domain (SD) field, but some are close to the multidomain (MD) region. Specimens with accepted results of palaeointensity are marked green, rejected are marked red. No systematic trend is observed between the position in the Day plot and the success in palaeointensity determination. Two specimens from MOB kiln have wasp-waisted hysteresis loops and therefore contain a considerable fraction of hematite. All other specimens plot close to lines determined by Dunlop (2002) for mixtures of SD and MD pure magnetite. As other ferromagnetic crystals are present in our samples, those experiments should be considered with caution.

For two specimens, first-order reversal curves (FORC) measurements have been carried out which demonstrate that the magnetic carriers are populations of MD and small PSD or SD grains (Fig. 5). According to Carvallo *et al.* (2006), SD particles are associated with closed concentric contours with a central peak in the FORC distribution. This is seen in the right diagram for the sister specimen of a successful Thellier experiment. Nevertheless there is also another fraction giving diverging contours along the H_b-axis and representing MD grains. For a sister specimen of a rejected Thellier experiment (left diagram) only open contours occur. Additionally, the vertical spread of the distribution indicates magnetostatically interacting grains.

5 DIRECTION AND STABILITY OF NRM

Although many specimens have scattered NRM directions a well-defined cluster can be seen at about 30° declination and 70° inclination (Fig. 6) for MOB and the inner part of kiln MOA (block samples 1–11). Samples from the outer part of MOA (12–29) and MOC show a considerable scatter and many aberrant directions. Such aberrant directions are very often correlated with low Q-factors.

AF demagnetization has been carried out for one specimen from each block representing various Koenigsberger ratios and also aberrant directions. Eight to 13 steps were performed in most cases with maximum fields of 120 mT. Additional thermal demagnetization of one specimen per block was performed for kiln MOA on chosen specimens with high Q-factor. Generally stable directions are observed, except for many specimens from the outer part of kiln MOA. Fig. 7 shows examples of demagnetization experiments. For MOA (Figs 7a and b) each orthogonal projection diagram shows a comparison of thermal and AF demagnetizations. In Fig. 7(a), two examples are shown which have no secondary component. Such a behaviour was found for three further specimens all coming from the inner part of the kiln MOA. Fig. 7(b) represents 12 specimens from the inner part and some from the outer part, which have only very weak secondary components removed by 10–20 mT or 150°C. Most specimens from the outer part showed an unstable behaviour or aberrant directions, and some had strong secondary components.

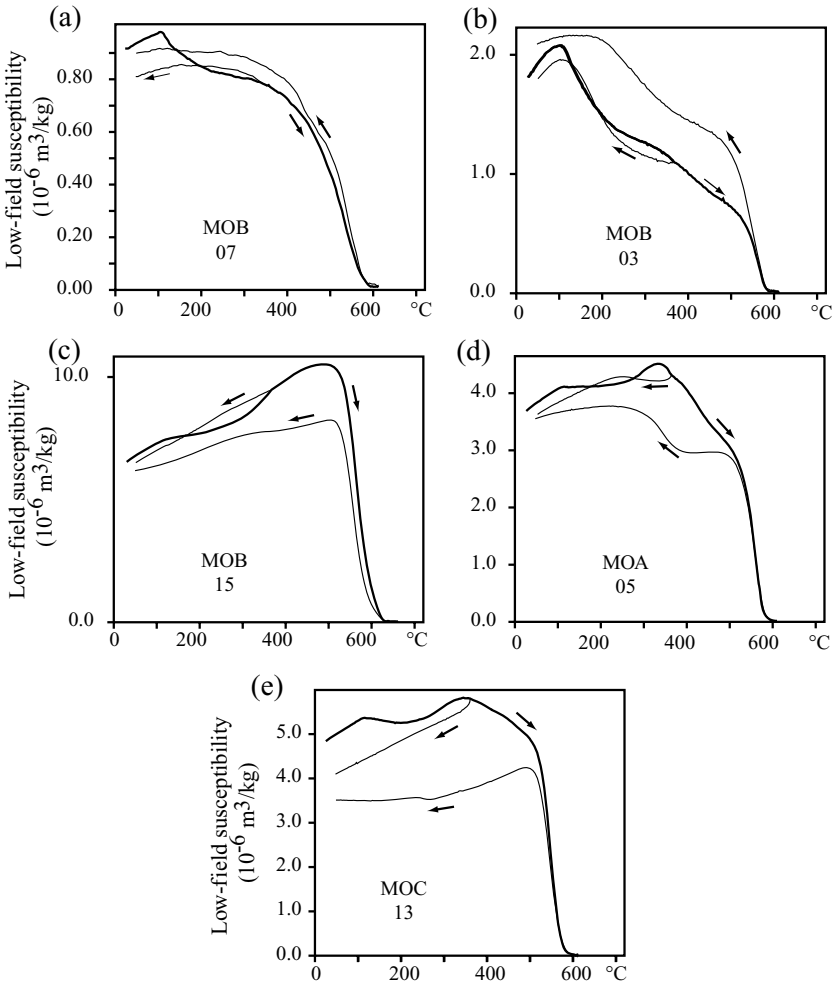

Figure 4. Examples of thermomagnetic curves: archaeointensity results of some sisters specimens are described later. Specimen (a) represents reliable archaeointensity results without mineralogical changes. Mineralogical alteration appears at 350–450°C for specimens (b), (c) and (d), but also before these temperatures, especially for specimens of kiln MOC (e).

Kiln MOB is characterized mainly by weak secondary components (Fig. 7c) and only three specimens needed more than 15 mT to reach the characteristic remanent magnetization (ChRM) direction. The resulting ChRM directions are well concentrated except for one outlier. Kiln MOC shows behaviour similar to MOA (Fig. 7d) with five specimens yielding no stable direction, secondary components removed after 20–25 mT on six specimens, and the rest of the samples with only weak secondary components (two examples are shown in Fig. 7d). The resulting ChRM directions are well concentrated except for one outlier.

Fig. 8(a) shows equal area projections of specimen ChRM directions for which principal component analysis (PCA, Kirschvink 1980) was possible. Some obvious aberrant ChRM directions (three from MOA with negative inclination and one from MOC with zero inclination) were not taken into account. Four specimens of MOA and MOC, respectively, did not allow application of PCA. While kilns MOB and MOC show well-concentrated archaeodirections, with only one outlier for MOC, the directions of MOA are much more scattered. To identify aberrant directions, which are caused by incomplete heating and/or inefficient demagnetization, an outlier test (McFadden 1982) was calculated for all directions (16) lying outside of the grey circle drawn in the diagram. This circle was drawn where most ChRM directions are concentrated. Eight directions were finally rejected.

The mean directions of the accepted ChRM directions were then derived for each sample block. Mean directions are shown in Fig. 8(b) and the highest scatter remains for kiln MOA. The structure mean directions and parameters of the Fisher statistics (Fisher 1953) are listed in Table 2. For MOB and MOC, higher precision parameters and smaller α_{95} radii have been obtained but the result from MOA can still be considered as reliable. To test, if these three directions are significantly different on a statistical basis, an *F*-test (McFadden & Lowes 1981) has been calculated and results are listed in Table 3. All three mean directions are significantly different, at the 95 per cent confidence level.

6 DETERMINATION OF ARCHAEOINTENSITY

The classical Thellier–Thellier protocol (Thellier & Thellier 1959) was only carried out on specimens whose AF or thermally demagnetized sisters-specimens presented a single component of magnetization. Almost all 46 specimens of the three kilns that were heated with a laboratory field applied along their *Z*-axis (i.e. along

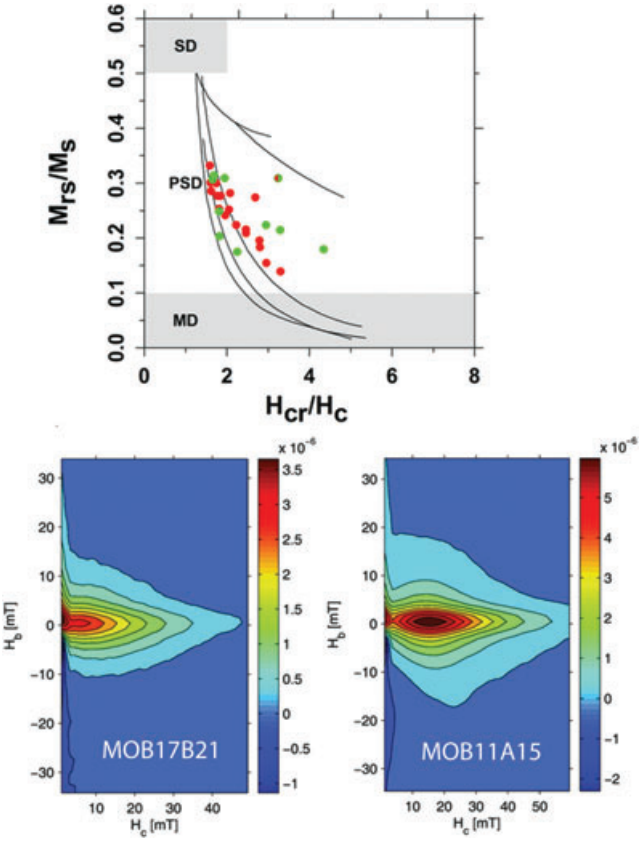

Figure 5. Day diagram (top panel): ratio of saturation magnetizations is plotted versus ratio of coercivities. The black lines were obtained according to Dunlop (2002) for mixtures of various amounts SD and SP (upper two curves) or MD magnetite (lower three curves). The successful outcome of Thellier experiments on sister specimens is indicated by green/red dots for accepted/rejected results. FORC diagrams (bottom panel) for two selected specimens from kiln MOB.

a subparallel direction to NRM) have positive pTRM checks. Following Chauvin *et al.* (2000), pTRM checks have been considered positive if, at a given temperature step, the difference between the original pTRM and the pTRM check does not exceed 10 per cent of the total TRM acquired. Positive pTRM checks should prove that specimens have not acquired a chemical remanent magnetization (CRM) during laboratory heating.

However, Fig. 9 illustrates the diversity of observed behaviours during the Thellier–Thellier experiments, especially for kiln MOC. Only a few specimens (24) presented the ideal linear behaviour on NRM–TRM diagrams, which is theoretically only observed for non-interacting SD grains (Thellier & Thellier 1959). The other specimens present strong concave-up behaviours (Fig. 9). In such cases, Chauvin *et al.* (2005) showed that widely different palaeointensities (overestimations or underestimations) could be obtained depending on which line segment is chosen.

Concavity cannot be explained by the existence of two components of magnetization. Moreover, high values of Koenigsberger ratio Q suggests that the magnetization is a TRM and not a thermochemical remanent magnetization (TCRM, see Fabian 2009).

The presence of PSD or MD grains (see e.g. Levi 1977; Coe *et al.* 2004; Chauvin *et al.* 2005; Dunlop *et al.* 2005; Biggin 2010) also results in concave-up NRM–TRM plots. Hysteresis results show the presence of a PSD or MD grain fraction, which could have affected the archaeointensity results. However, hysteresis properties studied

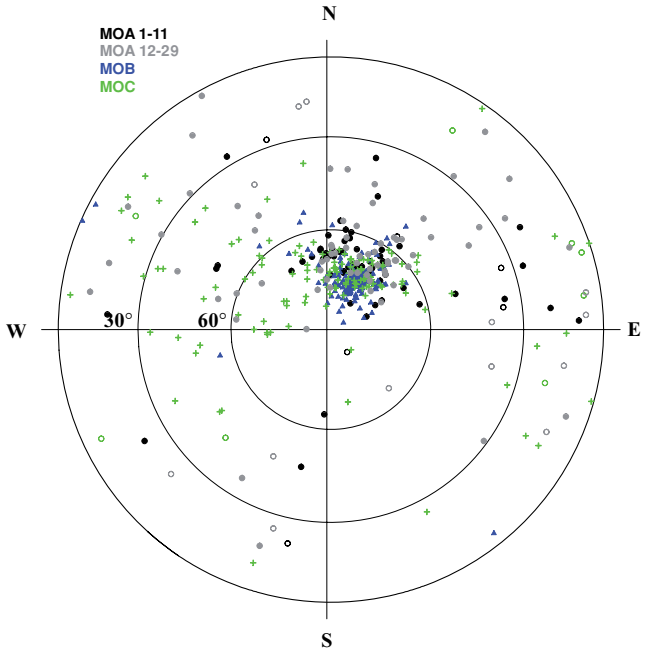

Figure 6. Directions of natural remanent magnetization (NRM) plotted in equal area projection. Kilns are indicated by different colours. Kiln MOA was divided into inner (block samples 1–11) and outer part (12–29).

for some sister-specimens do not show a systematic trend between linear/concave-up behaviour and position on the Day plot (Fig. 5). For MD grains, Biggin (2010) also observed no correlation between hysteresis results and concavity of NRM–TRM plots. FORC experiments show the difference in the grain assemblages for the linear and the concave-up Thellier experiments. Linear behaviour of the specimen (MOB17B21) is associated with SD particles. FORC distribution showing magnetostatically interacting grains correspond to a specimen with concave-up NRM–TRM plot (MOB11A15). In consequence, PSD–MD effects could explain non-ideal behaviour of some specimens, although these two examples are not sufficient to define a systematic trend. Moreover, numerous experimental and theoretical studies indicate that in the case of concave-up NRM–TRM diagrams induced by MD magnetic grains, the slope of the line through the initial and the final points yields the expected field strength (see e.g. Levi 1977; Fabian 2001; Coe *et al.* 2004; Chauvin *et al.* 2005). In Moyenvic samples, this approach yields a huge scatter of archaeointensities (30–110 μT) at the site level (Fig. 9), suggesting that curvature of NRM–TRM diagrams is not the result of MD magnetic grain effects.

Because thermomagnetic curves show strong alteration above 400 °C, concavity of NRM–TRM plots might be explained by mineralogical alteration, not detected by pTRM checks. CRM acquired during a Thellier experiment induces a deviation of NRM direction toward the laboratory field direction. However, if the laboratory field is subparallel to NRM, CRM acquisition may not cause a significant variation of NRM direction. Accordingly, 34 further Thellier experiments were carried out with a laboratory field of 70 μT applied along the X-axis of specimens, that is, quasi-perpendicular to NRM direction.

6.1 Angle between laboratory field and NRM

Fig. 10 presents two sisters-specimens heated with F_{Lab} applied along theirs Z (Fig. 10a) and X axes (Fig. 10b). For the latter, a

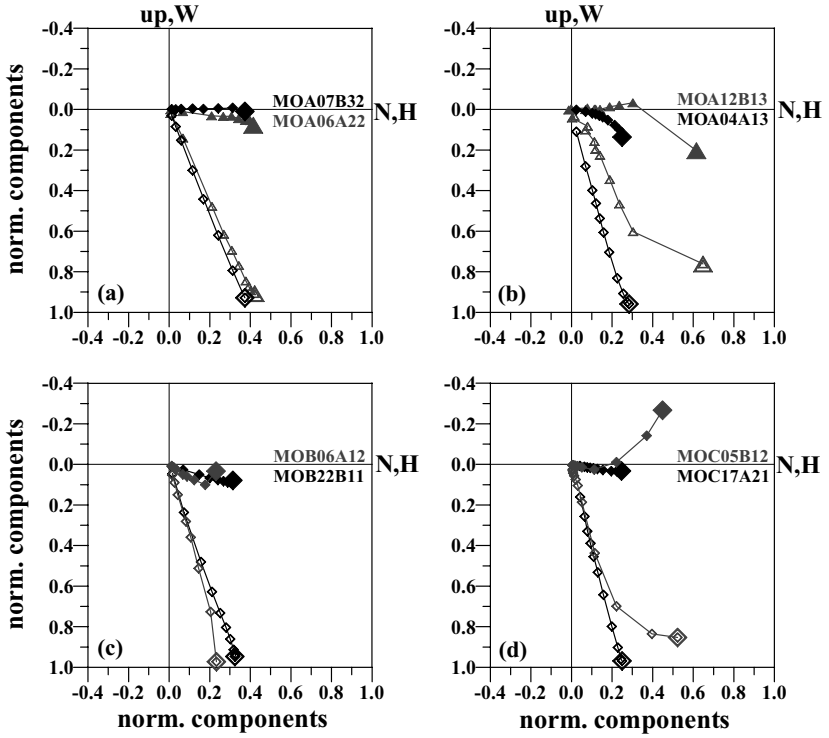

Figure 7. Demagnetization examples for kilns MOA (a and b), MOB (c) and MOC (d). Diagrams show normalized components of magnetization, triangles (diamonds) indicate thermal (AF) demagnetization. Closed (open) symbols are projection on the horizontal (vertical) plane (H corresponds to inclination). Specimen names are colour-coded to correspond to lines of the same colour in each diagram.

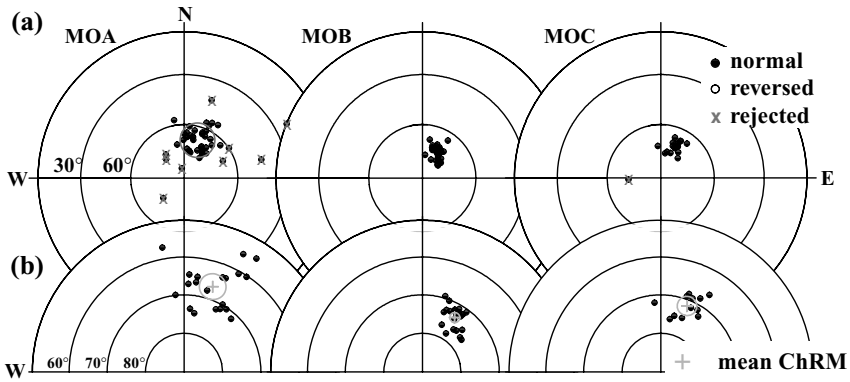

Figure 8. (a) Directions of characteristic remanent magnetization (ChRM) obtained from each thermal or AF demagnetization experiment plotted in equal area projection. For kiln MOA directions lying outside the grey circle were tested with the outlier test (McFadden & Lowes 1981), they are marked by a grey 'x', when rejected. (b) Mean ChRM directions. Black dots are mean directions of each block samples. The grey cross is the site-mean ChRM direction surrounded by the α_{95} circle in grey.

Table 2. Palaeomagnetic results of kilns from Moyenvic (48.780°N, 6.570°E): name, number of block samples, number of demagnetization experiments with alternating field (AF) or thermal (th), number of ChRM directions on block level, mean declination, inclination, precision parameter of Fisher statistics and radius α_{95} of error cone.

Abb.	n	AF/th	N	D (°)	I (°)	K	α_{95} (°)
MOA	29	26/21	20	18.6	66.6	92.0	3.4
MOB	23	30/4	22	30.9	73.6	538.2	1.3
MOC	18	16/3	12	21.8	71.6	306.8	2.5

Table 3. Results of the F-test (McFadden & Lowes 1981): combination of tested structures, parameter of f-distribution f_1 and f_2, significantly different on 95 per cent probability level, when $f_1 > f_2$.

Combination	f_1	f_2	Different?
MOA & MOB	0.394574	0.077769	Yes
MOA & MOC	0.158127	0.105014	Yes
MOB & MOC	0.153949	0.098139	Yes

strong deviation of the NRM direction toward that of the applied field is seen on the Zijderveld diagram and proves acquisition of a CRM during the Thellier experiment. CRM acquisition is also suggested by a weak deviation of the vertical component starting at 425°C for the other specimen from the same block (Fig. 10a), which presents the same variation of low-field susceptibility and decrease of NRM with temperature (Figs 10c and d). 18 specimens heated with $F_{\rm Lab}$ applied along their X-axis present the same deviation of the NRM direction. Accordingly, concave-up NRM–TRM diagrams are mostly explained by important mineralogical alteration, even

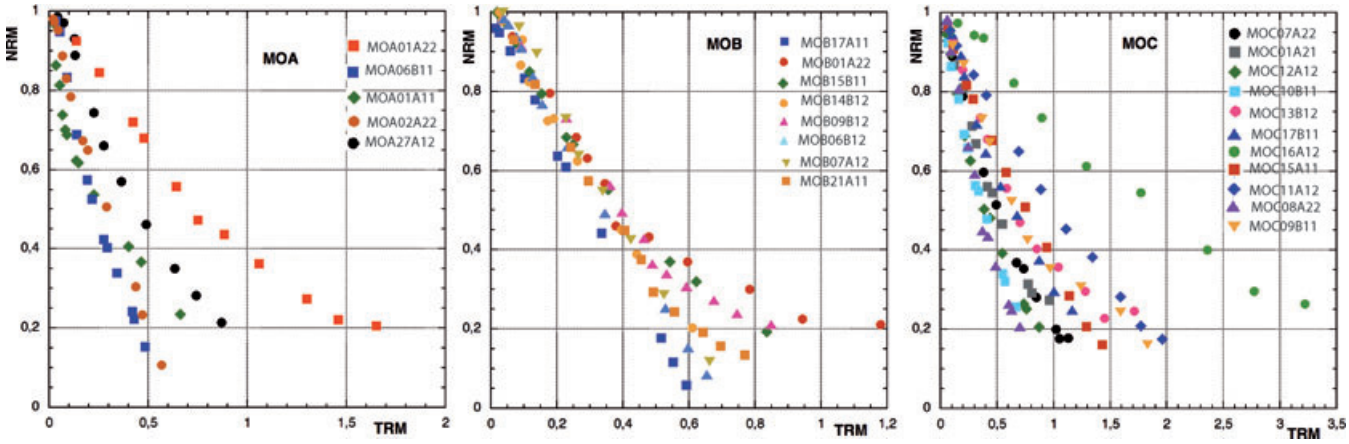

Figure 9. Composite NRM–TRM diagrams. Each panel shows the behaviour of samples (only with positive pTRM checks) from the same site (laboratory field 60 μT). In each composite Arai diagram, each symbol represents a particular specimen. Laboratory field was applied along the *Z*-axis of specimens.

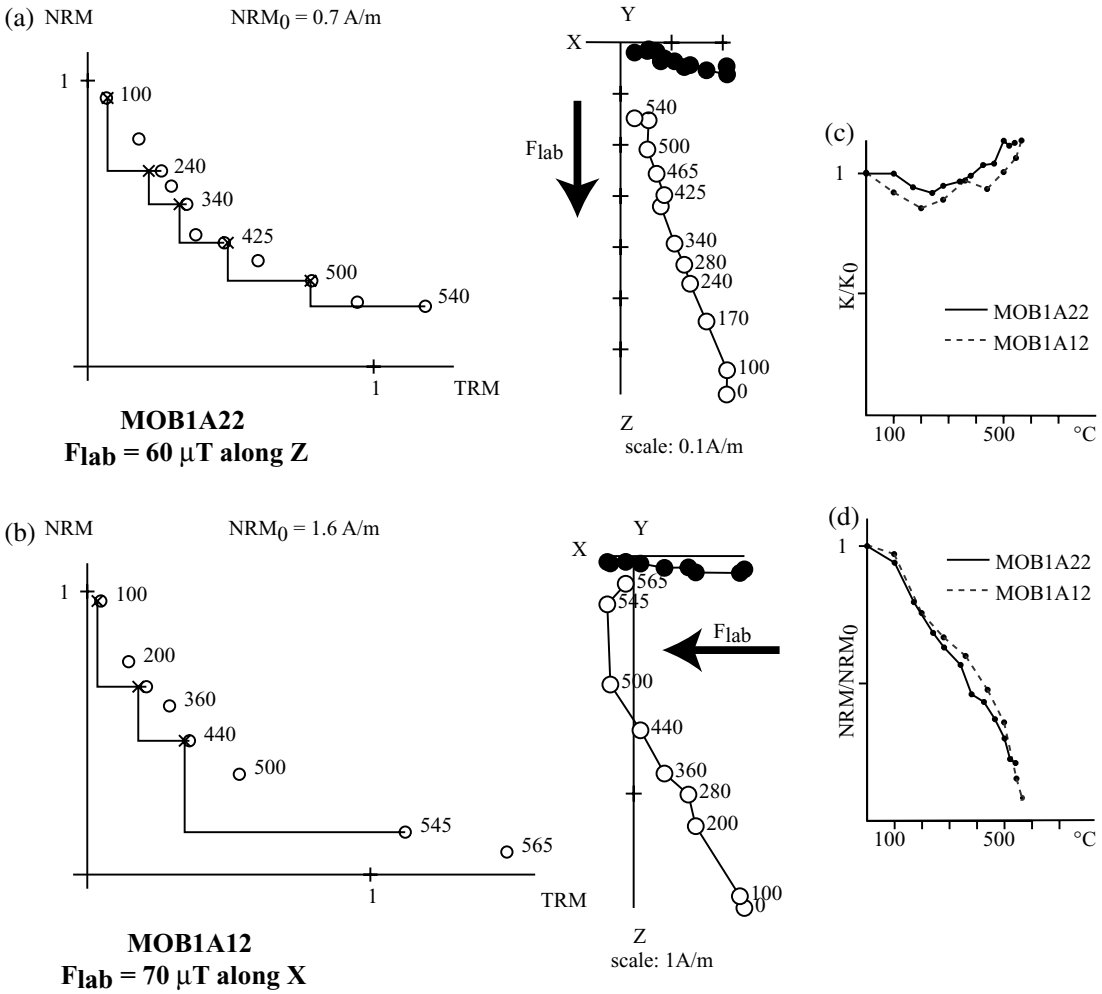

Figure 10. Comparison of NRM–TRM (left-hand side) and Zijderveld (middle) diagrams of sister's specimens heated with F_{Lab} applied along *Z*-axis (a) or *X*-axis (b) of the specimens. Directions in the Zijderveld diagrams are shown in specimen coordinates. Open (solid) circles are projections upon vertical (horizontal) planes. NRM–TRM diagrams are normalized to the initial NRM intensity. (c) Variation of low-field susceptibility for both specimens during successive heating steps. (d) NRM decrease with temperature for both specimens.

if neither negative pTRM checks nor high variation of low-field susceptibility have been observed.

Consequently, it was decided to retain only the specimens without significant deviation of their NRM directions toward that of the applied field. Mineralogical changes sometimes occurred from the first temperature steps (Fig. 10b); consequently, 35 specimens were rejected. The thermal stability of the specimens is lower than that expected according to the Koenigsberger ratio,

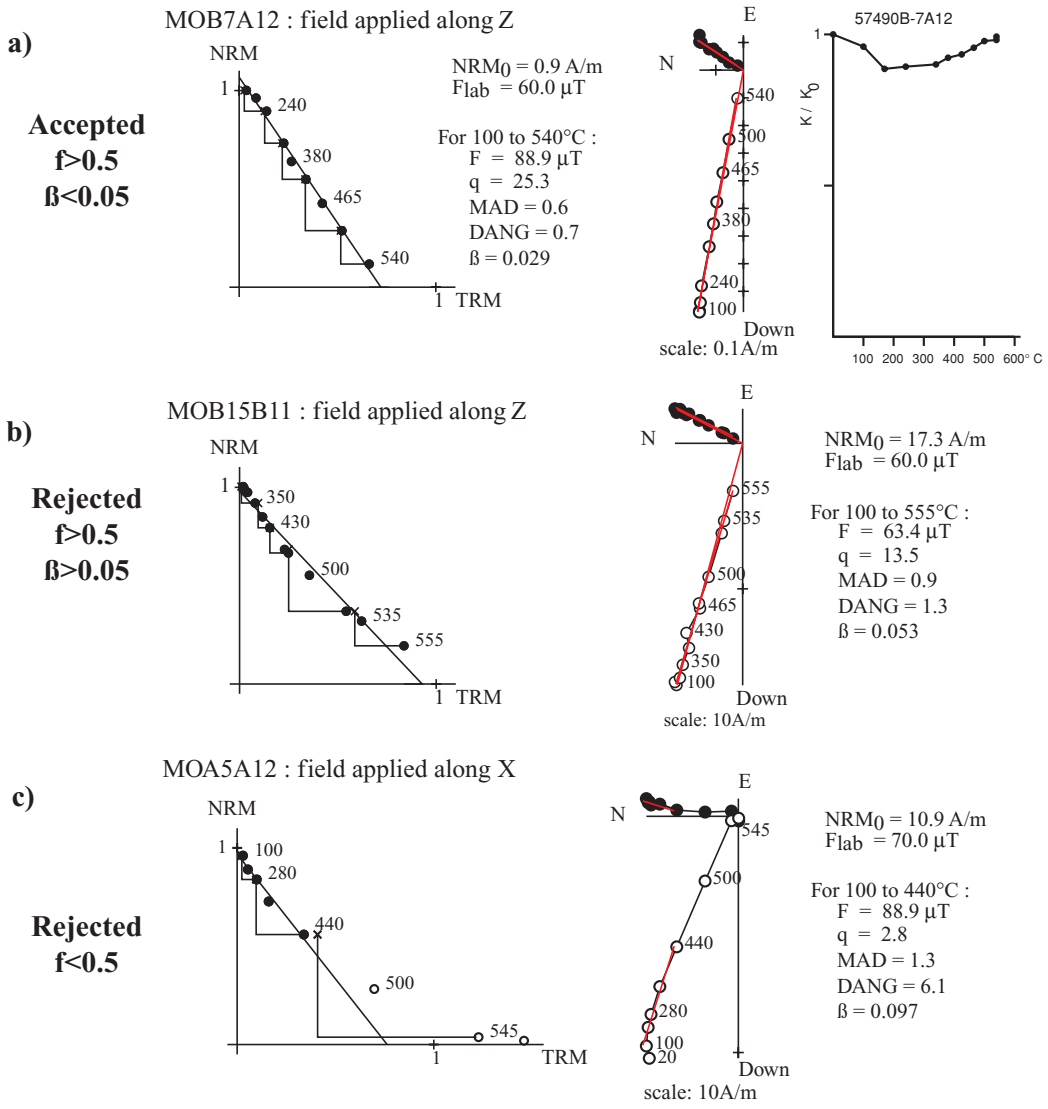

Figure 11. Examples of archaeointensity results for specimens that do not present significant deviation of NRM direction towards laboratory field direction. Directions on Zijderveld diagrams (right-hand side) are *in situ* coordinates. Open (solid) circles are projections upon vertical (horizontal) planes. NRM–TRM diagrams (left-hand side) are normalized to the initial NRM intensity. Variation of low-field susceptibility during successive heating steps is also provided in Fig. 11(a).

viscosity index and K-T experiments. This may be explained by an insufficient archaeological heating to stabilize magnetic mineralogy.

pTRM checks do not seem to be always sufficient criteria to detect mineralogical changes. Despite strong deviation of NRM direction, the fact that positive pTRM checks are observed may be explained by a low and continuous evolution at each temperature step. The best way to detect acquisition of a CRM seems to be the distortion of the NRM direction toward the laboratory field direction during successive heating steps. To be observed, this requires a large angular deviation between the applied F_{Lab} direction and the NRM direction.

6.2 Choice of criteria

Fig. 11 shows three examples of Thellier experiments on specimens for which no CRM acquisition is seen. Many authors (Biggin & Thomas 2003; Chauvin *et al.* 2005; Ben-Yosef *et al.* 2009) showed that a high NRM fraction (f factor, Coe *et al.* 1978) must be used to obtain reliable archaeointensity results. As recommended by Biggin & Thomas (2003) and Xu & Dunlop (2004), we rejected specimens with f values lower than 0.5 (Fig. 11c).

Three others parameters were used to select specimens with acceptable Thellier experiments. First, the maximum angular deviation (MAD, Kirschvink 1980), which measures the scatter in NRM directions, has to be lower than 5°. Second, the deviation angle (DANG, Selkin & Tauxe 2000) has to be also lower than 5°. However, it should be noted that the deviation angle is an inefficient rejection criterion if NRM direction and laboratory field are subparallel during the Thellier experiment. Third, we used β, the ratio of the standard error of the slope to the absolute value of the best-fit slope for the data on the NRM–TRM plot. An upper limit of 0.05 (Gee *et al.* 2010; Shaar *et al.* 2010) has been chosen (Fig. 11b) rather than 0.10 (Ben-Yosef *et al.* 2009) because specimens with ß higher than 0.05 (i.e. with slightly concave-up plots) tend to have scattered archaeointensities (Fig. 12).

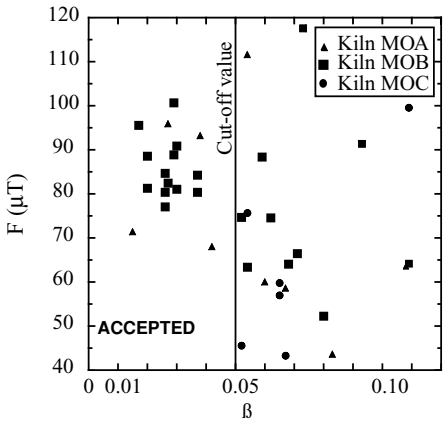

Figure 12. Distributions of archeointensities F versus ß (ratio of the standard error of the slope to the absolute value of the slope). Selected specimens do not present a strong distortion of NRM direction along laboratory field direction.

The chosen set of criteria (no significant deviation of NRM direction, positive pTRM checks, $f > 0.5$, MAD $< 5^\circ$, DANG $< 5^\circ$ and $\beta < 0.05$) finally led to the acceptance of linear NRM–TRM diagrams only (Fig. 11a**)**, that is, four specimens of kiln MOA, 12 of MOB and none of MOC (Table 4). The rejection rates of this study are thus very high (88 per cent for kiln MOA, 73 per cent for MOB and 100 per cent for MOC), but all the accepted data have high quality factor q (Coe *et al.* 1978) ranging from 10 to 50.

6.3 Archaeointensity results

Table 4 shows that archaeointensities determined on specimens heated with $F_{\rm Lab}$ applied along their X-axis are slightly, but systematically lower than those obtained on sister-specimens with $F_{\rm Lab}$ applied along their Z-axis. This could be explained by TRM anisotropy. As mean archaeointensities were computed using all specimens heated with laboratory field along Z- or X-axis, TRM anisotropy is taken account. Because specimens are prone to alteration it seems unlikely that TRM anisotropy checks would significantly reduce the scatter around mean archaeointensities per site.

The mean archaeointensity per site was determined using the weighting factor proposed by Prévot *et al.* (1985). This gives an archaeointensity weighted mean of 80.1 ± 14.5 μT for kiln MOA and 86.6 ± 6.9 μT for kiln MOB (Table 4). Considering the strong magnetic physicochemical changes of the specimens during heating steps, cooling-rate corrections were not performed.

7 RESULTS

Site-mean directions and available directional reference data, all relocated to Paris by Virtual Geomagnetic Poles (VGP), were compared (Fig. 13). Inclination and declination results are consistent with the French (Gallet *et al.* 2002) and the Bayesian German (Schnepp & Lanos 2005) archaeomagnetic secular variation curves. Apparent discrepancies in inclination between MOA and MOB sites and the French curve are probably due to the low number of published reference sites.

Table 4. Archeointensity results. Kiln name; block sample number; specimen name; intensity of initial NRM; initial low-field susceptibility (10^{-6} SI); field: direction of laboratory field along Z- or X-axis of specimen; $T_{\rm min} - T_{\rm max}$: temperature interval used to determine intensity; $F \pm \sigma$: archaeointensity with associated standard deviation; n: number of heating steps within $T_{\rm min} - T_{\rm max}$ interval; MAD: maximum angular deviation; DANG: deviation angle; f: NRM fraction; g : gap factor; q: quality factor (Coe *et al.* 1978); ß : ratio of the standard error of the slope to the absolute value of the slope; $F_{\rm mean}$: arithmetic average; $F_{\rm w}$: weighted mean archaeointensity (Prévot *et al.* 1985); σ : standard deviation; VDM (VADM): virtual (axial) dipole moment.

Kiln	Sample	Specimen	NRM (A m^{-1})	K	Field	$T_{\rm min} - T_{\rm max}$(°C)	$F \pm \sigma$ (μT)	n	MAD (°)	DANG (°)	f	g	q	ß
MOA	2	MOA02A12	12.0	6.9	X	100 – 565	93.2 ± 3.5	8	2.0	1.5	1.01	0.76	20.3	0.038
	2	MOA02A22	11.3	7.6	Z	100 – 555	95.9 ± 2.6	12	1.3	1.5	0.88	0.85	27.6	0.027
	6	MOA06B22	1.6	1.6	X	100 – 565	71.4 ± 1.1	8	1.2	0.9	0.92	0.83	49.4	0.015
	27	MOA27A11	2.6	4.1	X	100 – 440	68.0 ± 2.9	5	1.6	4.5	0.64	0.66	10.0	0.042
						$F_{\rm mean} + \sigma = 82.1 \pm 14.5$ μT								
						$F_{\rm w} \pm \sigma = 80.1 \pm 14.5$ μT								
						VADM = 12.6 (10^{22} A m^2)								
						VDM = 12.6 (10^{22} A m^2)								
MOB	6	MOB06B11	2.8	3.5	X	100 – 565	81.3 ± 1.6	8	1.6	0.7	0.93	0.76	35.2	0.020
	6	MOB06B12	2.1	2.4	Z	100 – 540	88.6 ± 1.8	11	0.9	0.3	0.88	0.84	36.7	0.020
	7	MOB07A12	0.9	1.6	Z	100 – 540	88.9 ± 2.6	9	0.6	0.7	0.85	0.86	25.3	0.029
	9	MOB09B11	7.6	6.6	Z	100 – 555	100.7 ± 2.9	12	1.0	0.8	0.66	0.88	20.0	0.029
	9	MOB09B21	5.8	6.6	X	100 – 565	81.1 ± 2.4	8	1.4	1.0	0.82	0.82	22.5	0.030
	10	MOB10B11	3.2	6.4	Z	100 – 465	82.5 ± 2.2	7	1.0	2.2	0.54	0.82	16.4	0.027
	13	MOB13B21	21.1	28.8	Z	100 – 555	80.4 ± 3.0	12	0.6	0.9	0.73	0.81	15.6	0.037
	14	MOB14B11	16.9	12.5	X	100 – 565	77.1 ± 2.0	8	1.0	0.2	0.85	0.75	24.5	0.026
	14	MOB14B12	20.5	18.8	Z	100 – 555	84.3 ± 3.1	12	1.8	2.3	0.80	0.84	18.0	0.037
	17	MOB17A11	22.3	9.1	Z	100 – 555	95.6 ± 1.6	12	0.8	0.5	0.92	0.83	46.5	0.017
	17	MOB17A12	24.1	9.4	X	100 – 565	90.9 ± 2.7	8	1.2	0.7	1.00	0.71	23.4	0.030
	21	MOB21A11	0.3	0.7	Z	100 – 465	84.7 ± 2.2	8	1.2	1.2	0.68	0.84	22.1	0.026
						$F_{\rm mean} \pm \sigma = 86.3 \pm 6.9$ μT								
						$F_{\rm w} \pm \sigma = 86.6 \pm 6.9$ μT								
						VADM = 13.6 (10^{22} A m^2)								
						VDM = 12.4 (10^{22} A m^2)								

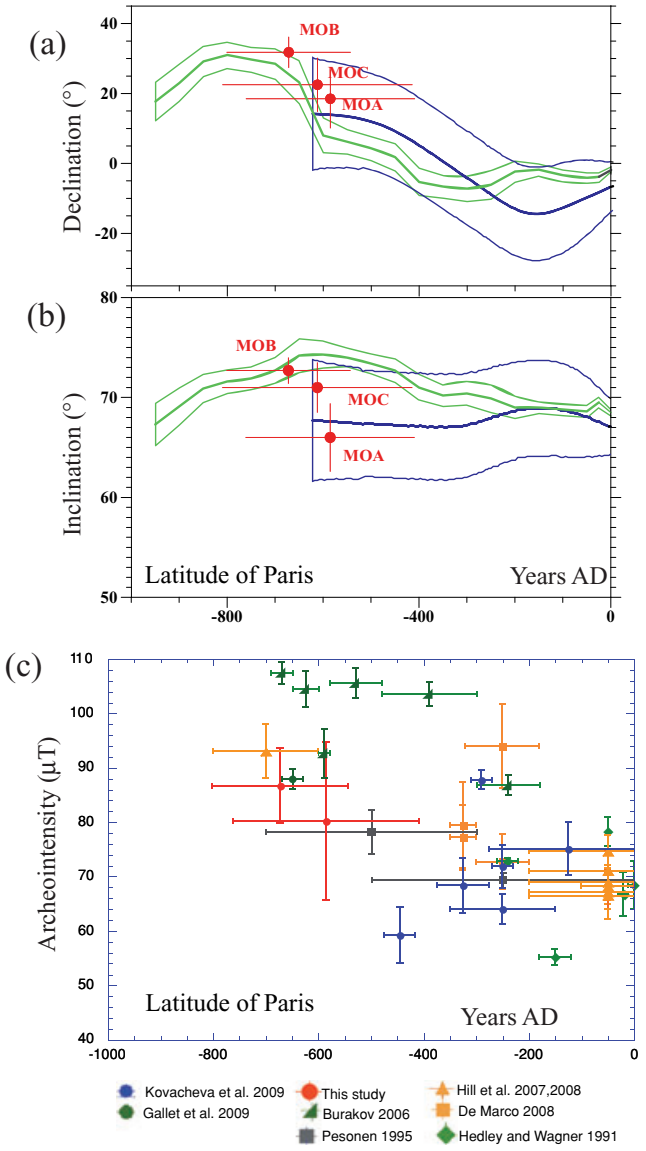

Figure 13. Comparison of Moyenvic declination (a), inclination (b) and archaeointensity (c) with archaeodirections reference curves of France (green) and Germany (blue) or sites from Europe. Archaeointensities based on Thellier's method with pTRM checks only. Data are relocated to Paris (48.85°N, 2.30°E), via VGP for directional data and VADM for archaeointensity data.

No archaeointensity reference curve is yet published for protohistoric times in western Europe. Data acquired with the Thellier method, including pTRM checks and anisotropy corrections, are only available for France (Hedley & Wagner 1991), Switzerland (Kovacheva 2009), Mediterranean Europe and Finland (Pesonen *et al.* 1995). These published data were corrected for anisotropy using either TRM or magnetic susceptibility (AMS) or anhysteric remanent magnetization (ARM) or IRM. Only data published by Hill *et al.* (2007, 2008), De Marco (2008) and Gallet *et al.* (2009), were corrected for TRM anisotropy and cooling rate effects. Our archaeointensity results are consistent (Fig. 13c) with Italian (Hill *et al.* 2008; Gallet *et al.* 2009) data. The Spanish data (Burakov *et al.* 2006) obtained from potsherds present somewhat higher values that could be explained by the fact that their data were corrected for anisotropy using AMS which give usually a lower correcting factor than TRM anisotropy (Chauvin *et al.* 2000). Moreover cooling-rate effects were not corrected for these data but are relevant for such material (Genevey & Gallet 2002). Finally, discrepancies between data in Fig. 13(c) could be explained by some dating inaccuracy and/or differences in the methods used to correct for anisotropy and cooling rate effect. However our new data confirm high archaeointensity values (about twice the present day field value) during the first half of the Early Iron Age.

8 CONCLUSION

In this study a full magnetic field vector analysis was performed on three salt kilns from Moyenvic (East France), dated by radiocarbon analysis on charcoals. The mean archaeomagnetic directions were obtained after thermal and AF demagnetizations and the original Thellier method was used to obtain high-quality archaeointensity results. The interpretation of the archaeointensity experiments, performed on 80 samples, was particularly complex. This might be explained by insufficient archaeological heating to stabilize magnetic mineralogy, a common situation on archaeomagnetic sites from the first millennium BC. 75 per cent of the studied specimens present concave-up NRM–TRM plots with positive pTRM checks, a behaviour commonly attributed to coarse grains effects predicted by hysteresis and FORC analysis. However, PSD–MD grains effects do not seem the main cause of failures of the palaeointensity experiments. The obvious distortion of NRM direction towards the laboratory field direction proves the occurrence of strong mineralogical alteration, not detected by pTRM checks. Moreover, for similar large f factors, archaeointensities of concave-up plots are significantly lower than archaeointensities of linear NRM–TRM plots, which would not be expected for MD grains.

Consequently, we advise to apply the laboratory field in a direction at a large angle from that of the NRM, to detect mineralogical alterations and, ultimately, to avoid the incorrect interpretation of concavity on NRM–TRM plots as only due to coarse grains effects.

High values of eastern declination and strong field archaeointensities were obtained, providing further evidence for important changes of the Earth's magnetic field in Europe during first half of the first millennium BC.

This study provides new reliable reference data for the data sets of Germany and France. Further studies have to be carried out for the first millennium BC, to better characterize these strong variations of the Earth's magnetic field. Such variations suggest that archaeomagnetism would provide an effective tool to date accurately archaeological structures of the Early Iron Age, especially during the long plateau found in the radiocarbon calibration curve (Hajdas 2008) lasting from 750 to 400 BC.

ACKNOWLEDGMENTS

J.D. Laffitte (INRAP) is kindly acknowledged for providing archaeological information about the site and the kilns. We thank Philippe Dufresne for his help during sampling and sample preparation, Guillame Dupont-Nivet for his attentive reading and Pierrick Roperch for helpful and animated discussions. Dry cutting of the B-slices and demagnetization of strong B-specimens have been carried out in the Palaeomagnetic Laboratory of the LIAG (Hannover), Christian Rolf is kindly acknowledged for his support. E.S. has been supported by the Austrian science fund FWF grant P19370-N19. This

work was partly financed by the CNRS/INSU Paléo2 programme. We are grateful to Jan Hus and an anonymous reviewer for their constructive comments on this paper.

REFERENCES

Ben-Yosef, E., Tauxe, L., Levy, T.E., Shaar, R., Ron, H. & Najjar, M., 2009. Geomagnetic intensity spike recorded in high resolution slag deposit in Southern Jordan, *Earth planet. Sci. Lett.*, **287,** 529–539, doi:10.1016/j.epsl.2009.09.001.

Bertaux, J.P., 1987. La fabrication du sel à l'époque protohistorique par la technique du briquetage, in *L'Âge du Fer en Lorraine*, pp. 85–100, Musée de Sarreguemines, Sarreguemines.

Biggin, A.J., 2010. Are systematic differences between thermal and microwave Thellier-types palaeointensity estimates a consequence of multidomain bias in the thermal results?, *Phys. Earth planet. Inter.*, **280,** 16–40, doi:10.1016/j.pepi.2010.03.005.

Biggin, A.J. & Thomas, D.N., 2003. The application of acceptance criteria to results of Thellier palaeointensity experiments performed on samples with pseudo-single-domain-like chararcteristics, *Phys. Earth planet.Inter.,* **138,** 279–287.

Bronk Ramsey, C., 2005. Improving the resolution of radiocarbon dating by statistical analysis, in: *The Bible and Radiocarbon Dating: Archaeology, Text and Science*, pp. 57–64, eds Levy, T.E. & Higham, T.F.G., Equinox, London.

Burakov, K.S., Nachasova, I.E. & Mata, C., 2006. Geomagnetic field intensity in the first millenium BC from data on ceramics of the Los Villares archaeological monument (Spain), *Fizika Zemli,* **11,** 84–92. [Izvestiya Physics of the Solid Earth, 42(11), 942–950].

Carvallo, C., Roberts, A.P., Leonhardt, R., Laj, C., Kissel, C. & Camps, P., 2006. Increasing the efficiency of palaeointensity analyses by selection of samples using first-order reversal curve diagrams, *J. geophys. Res.,* **111,** B12103, doi:10.1029/2005JB004126.

Chauvin, A., Garcia, Y., Lanos, Ph. & Laubenheimer, F., 2000. Palaeointensity of the geomagnetic field recovered on archaeomagnetic sites from France, *Phys. Earth planet.Inter.,* **120,** 111–136.

Chauvin, A., Roperch, P. & Levi, S., 2005. Reliability of geomagnetic palaeointensity data : the effects of the NRM fraction and concave-up behaviour on palaeointensity determinations by the Thellier method, *Phys. Earth planet.Inter.,* **150,** 265–286.

Coe, R.S., Gromme, S. & Mankinen, E.A., 1978. Geomagnetic palaeointensities from radiocarbon-dated lava flows on Hawaii and the question of the Pacific non-dipole low, *J. geophys. Res.,* **83,** 1740–1756.

Coe, R.S., Riisager, J., Plenier, G., Leonhardt, R. & Krasa, D., 2004. Multidomain behaviour during palaeointensity experiments: results from the 1915 Mt Lassen flow, *Phys. Earth planet.Inter.,* **147,** 141–153.

Daire, M.Y., 2003. *Le sel des Gaulois*, p. 152, Errance, Paris.

Day, R., Fuller, M. & Schmidt, V.A., 1977. Hysteresis properties of titanomagnetites, grain size and compositional dependence, *Phys. Earth planet.Inter.,* **13**(4), 260–267.

De Marco, E., Spataras, V., Gomez-Paccard, M., Chauvin, A. & et Kondopoulou, D., 2008. New archaeointensity results from archaeological sites and variation of the geomagnetic field intensity for the last 7 millenia in Greece, *Phys. Chem. Earth,* **33**(6–7), 578–595.

Dunlop, D., 2002. Theory and application of the day plot (Mrs/Ms versus Hcr/Hc), 2: application to data for rocks, sediments and soils, *J. geophys. Res.,* **107**(B3), EPM 5-1–EMP 5-15.

Dunlop, D.J., Zhang, B. & Özdemir, Ö., 2005. Linear and nonlinear Thellier palaeointensity behaviour of natural minerals, *J. geophys. Res.,* **110,** B01103, doi:10.1029/2004JB003095.

Fabian, K., 2001. A theoretical treatment of palaeointensity determination experiments on rocks containing pseudo-single or multi domain magnetic particles, *Earth planet. Sci. Lett.,* **168,** 45–58.

Fabian, K., 2009. Thermochemical remanence acquisition in single-domain particle ensembles: a case for possible overestimation of the geomagnetic palaeointensity, *Geochem. Geophys. Geosyst.,* **10,** Q06Z03, doi:10.1029/2009GC002420.

Fisher, R.A., 1953. Dispersion on a sphere, *Proc. R. Soc. Lond.,* **A-127**, 295–305.

Gallet, Y., Genevey, A. & Le Goff, M., 2002. Three millenia of directional variation of the Earth's magnetic field in western Europe as revealed by archeological artefacts, *Phys. Earth planet.Inter.,* **131,** 81–89.

Gallet, Y., Genevey, A., Le Goff, M., Warmé, N., Gran-Aymerich, J. & Lefèvre, A., 2009. On the use of archaeology in geomagnetism, and vice-versa: recent developments in archeomagnetism, *C.R. Physique*, **10,** 630–648, doi:10.1016/j.crhy.2009.08.005.

Gee, J.S., Yu, Y. & Bowles, J., 2010. Palaeointensity estimates from ignimbrites: an evaluation of the Bishop Tuff, *Geochem. Geophys. Geosyst.*, **11,** Q10007, doi:10.1029/2009GC002888.

Genevey, A. & Gallet, Y., 2002. Intensity of the geomagnetic field in Western Europe over the past 2000 years: new data from ancient French pottery, *J. geophys. Res.,* **107**(B11), 2285, doi:10.1029/2001JB000701.

Genevey, A., Gallet, Y., Rosen, J. & Le Goff, M., 2009. Evidence of rapid geomagnetic field intensity variation in western Europe over the past 800 years from new French archeointensity data, *Earth planet. Sci. Lett.,* **202**(1–2), 132–143.

Gomez-Paccard, M. et al. & Archeological working group, 2006. A catalogue of Spanish archaeomagnetic data, *Geophys. J. Int.,* **166,** 1125–1143.

Gomez-Paccard, M., Chauvin, A., Lanos, P. & Thiriot, J., 2008. New archeointensity data from Spain and the geomagnetic dipole moment in western Europe over the past 2000 years, *J. geophys. Res.,* **113,** B09103, doi:10.1029/2008JB005582.

Hajdas, I., 2008. Radiocarbon dating and its applications in Quaternary studies / Die Radiokohlenstoffmethode und ihre Anwendung in der Quartärforschung, *Quaternary Sci. J. (Eiszeitalter und Gegenwart),* **57**(1–2), 2–24.

Hedley, I. & Wagner, G.C., 1991. A magnetic investigation of roman and pre-roman pottery, in *Archaeometry '90*, pp. 275–284, eds Pernicka, E. & Wagner, G.C., Birkhauser Verlag, Basel.

Hill, M.J., Lanos, P., Chauvin, A., Vitali, D. & Laubenheimer, F., 2007. An archeomagnetic investigation of a roman amphorae workshop in Albinia, *Geophys. J. Int.,* **169**(2), 471–472.

Hill, M.J., Lanos, P., Denti, M. & Dufresne, P., 2008. Archeomagnetic investigation of bricks from the VIII century BC Greek-indigenous site of Incoronata (Metaponto, Italy), *Phys. Chem. Earth,* **33**(6–7), 523–533, doi:10.1016/j.pce.2008.02.026.

Kirschvink, J.L., 1980. The least-squares line and plane and the analysis of palaeomagnetic data, *Geophys. J. R. astr. Soc.,* **62,** 699–718.

Kovacheva, M., Boyadziev, Y., Kostadinova-Avramova, M., Jordanova, N. & Donadini, F., 2009. Updated archeomagnetic data set of the past 8 millennia from the Sofia laboratory, *Geochem. Geophys. Geosyst.,* **10,** Q05002, 6PP, doi:10.1029/2008GC002347.

Korte, M, Donadini, F & Constable, C.G., 2009. Geomagnetic field for 0–3 ka: 2. A new series of time-varying global models, *Geochem. Geophys. Geosyst.,* **10,** Q06008, doi:10.1029/2008GC002297.

Laffitte, J.D., 2002. Le briquetage de la Seille à Moyenvic (Moselle, France) au lieu-dit Les Crôleurs, in *Archéologie du sel, Techniques et sociétés dans la Pré et Protohistoire européenne*, pp. 197–207, ed. Weller, O., Actes du XIV^{e} Congrès UISPP de Liège, Verlag Marie Leidorf, Rahden/Westfalen.

Lanos P., 2004. Bayesian inference of calibration curves, application to archaeomagnetism: chapter 3, in *Tools for Constructing Chronologies, Crossing Disciplinary Boundaries,* Lecture Notes in Statistics, Vol. 177, pp. 43–82, eds, Buck, C.E. & Millard, A.R., Springer-Verlag, London.

Levi, S., 1977. The effect of magnetite particle size on palaeointensity determinations of the geomagnetic field, *Phys. Earth planet.Inter.,* **13,** 245–259.

McFadden, P.L., 1982. Rejection of palaeomagnetic observations, *Earth planet. Sci. Lett.,* **61,** 392–395.

McFadden, P.L. & Lowes, F.J., 1981. The discrimination of mean directions drawn from Fisher distributions, *Geophys. J.,* **67,** 19–33.

Pavon-Carrasco, F.J., Osete, M.L., Torta, J.M. & Gaya-Piqué, L.R., 2009. A regional archeomagnetic model for Europe for the last 3000 years,

SCHA.DIF.3k: applications to archeomagnetic dating, *Geochem. Geophys. Geosyst.,* **10,** Q03013, doi:10.1029/2008GC002244.

Pesonen, L.J., Leino, M.A.H. & Nevanlinna, H., 1995. Archeomagnetic intensity in Finland during the last 6400 years: evidence for a latitude-dependant nondipole field at approximate AD 500, *J. Geomagn. Geoelectr.,* **47,** 19–40.

Pike, C.R., Roberts, A.P. & Verosub, K.L., 1999. Characterizing interactions in fine magnetic particle systems using first order reversal curves, *J. appl. Phys.,* **85,** 6660–6667.

Prévot, M., Mankinen, E.A., Coe, R.S. & Gromme, C.S., 1985. The Steens Mountain (Oregon) geomagnetic polarity transition, 2. Field intensity variations and discussion of reversal models, *J. geophys. Res.,* **90**(B12), 10 417–10 448.

Reimer, P.J. *et al.,* 2004. IntCal04 terrestrial radiocarbon age calibration, 0–26 cal kyr BP, *Radiocarbon,* **46**(3), 1029–1058.

Roberts, A.P., Pike, C.R. & Verosub, K.L., 2000. FORC diagrams: a new tool for characterizing the magnetic properties of natural samples, *J. geophys. Res.,* **105**(28), 461–475.

Schnepp, E. & Lanos, P., 2005. Archaeomagnetic secular variation in Germany during the past 2500 years, *Geophys. J. Int.,* **163,** 479–490.

Schnepp, E., Lanos, P. & Chauvin, A., 2009. Geomagnetic palaeointensity between 1300 and 1750 A.D. derived from a bread floor sequence in Lübeck, Germany, *Geochem. Geophys. Geosyst.,* **10,** Q08003, doi:10.1029/2008GC002470.

Selkin, P.A. & Tauxe, L., 2000. Long-term variations in palaeointensity, *Phil. Trans. R. Soc. Lond. A,* **358,** 1065–1088.

Shaar, R., Ron, H., Tauxe, L., Kessel, R., Agnon, A., Ben-Yosef, E. & Feinberg, J.M., 2010. Testing the accuracy of absolute intensity estimates of the ancient geomagnetic field using copper slag material, *Earth planet. Sci. Lett.*, **290,** 201–213, doi:10.1016/j.epsl.2009.12.022.

Tema, E., Hedley, I. & Lanos, P., 2006. Archaeomagnetism in Italy: a compilation of data including new results and a preliminary Italian secular variation curve, *Geophys. J. Int.,* **167,** 1160–1171.

Thellier, E. & Thellier, O., 1944. Recherches géomagnetiques sur des coulées volcaniques d'Auvergne, *Ann. Geophys.,* **1,** 37–52.

Thellier, E. & Thellier, O., 1959. Sur l'intensité du champ magnétique terrestre dans le passé historique et géologique, *Ann. Geophys.,* **15,** 285–376.

Xu, S. & Dunlop, D.J., 2004. Thellier palaeointensity theory and experiments for multidomain grains, *J. geophys. Res.,* **109,** B07103, doi:10.1029/2004JB003024.

Zananiri, I., Batt, C.M., Lanos, P., Tarling, D.H. & Linford, P., 2007. Archaeomagnetic secular variation in the UK during the past 4000 years and its application to archaeomagnetic dating, *Phys. Earth planet.Inter.,* **160,** 97–107.